BBA - General Subjects 1867 (2023) 130419

Contents lists available at ScienceDirect

BBA - General Subjects

journal homepage: www.elsevier.com/locate/bbagen

Subunit composition of mitochondrial dehydrogenase complexes in diplonemid flagellates

Kristína Záhonová [a,b,c,d,1], Matus Valach [e,1], Pragya Tripathi [a,f,1], Corinna Benz [a], Fred R. Opperdoes [g], Peter Barath [h,i], Veronika Lukáčová [i], Maksym Danchenko [h], Drahomíra Faktorová [a,f], Anton Horváth [j], Gertraud Burger [e], Julius Lukeš [a,f,*], Ingrid Škodová-Sveráková [a,b,j,*]

[a] Institute of Parasitology, Biology Centre, Czech Academy of Sciences, České Budějovice (Budweis), Czech Republic
[b] Life Science Research Centre, Faculty of Science, University of Ostrava, Ostrava, Czech Republic
[c] Department of Parasitology, Faculty of Science, Charles University, BIOCEV, Vestec, Czech Republic
[d] Division of Infectious Diseases, Department of Medicine, University of Alberta, Edmonton, Canada
[e] Department of Biochemistry and Robert-Cedergren Centre for Bioinformatics and Genomics, Université de Montréal, Montreal, Canada
[f] Faculty of Sciences, University of South Bohemia, České Budějovice (Budweis), Czech Republic
[g] de Duve Institute, Université Catholique de Louvain, Brussels, Belgium
[h] Institute of Chemistry, Slovak Academy of Sciences, Bratislava, Slovakia
[i] Medirex Group Academy, Nitra, Slovakia
[j] Faculty of Natural Sciences, Comenius University, Bratislava, Slovakia

ARTICLE INFO

Keywords:
Dehydrogenase complexes
Evolution
Diplonema papillatum
Diplonemids
Protist
Mitochondrion

ABSTRACT

In eukaryotes, pyruvate, a key metabolite produced by glycolysis, is converted by a tripartite mitochondrial pyruvate dehydrogenase (PDH) complex to acetyl-coenzyme A, which is fed into the tricarboxylic acid cycle. Two additional enzyme complexes with analogous composition catalyze similar oxidative decarboxylation reactions albeit using different substrates, the branched-chain ketoacid dehydrogenase (BCKDH) complex and the 2-oxoglutarate dehydrogenase (OGDH) complex. Comparative transcriptome analyses of diplonemids, one of the most abundant and diverse groups of oceanic protists, indicate that the conventional E1, E2, and E3 subunits of the PDH complex are lacking. E1 was apparently replaced in the euglenozoan ancestor of diplonemids by an AceE protein of archaeal type, a substitution that we also document in dinoflagellates. Here, we demonstrate that the mitochondrion of the model diplonemid *Paradiplonema papillatum* displays pyruvate and 2-oxoglutarate dehydrogenase activities. Protein mass spectrometry of mitochondria reveal that the AceE protein is as abundant as the E1 subunit of BCKDH. This corroborates the view that the AceE subunit is a functional component of the PDH complex. We hypothesize that by acquiring AceE, the diplonemid ancestor not only lost the eukaryotic-type E1, but also the E2 and E3 subunits of the PDH complex, which are present in other euglenozoans. We posit that the PDH activity in diplonemids seems to be carried out by a complex, in which the AceE protein partners with the E2 and E3 subunits from BCKDH and/or OGDH.

1. Introduction

Pyruvate is made from two main energy sources, carbohydrates and amino acids. Pyruvate dehydrogenase (PDH) is a multi-enzyme complex that controls the entry of pyruvate into the tricarboxylic acid (TCA) cycle [1]. PDH not only decarboxylates pyruvate as its name suggests but transforms it into acetyl-coenzyme A (CoA), CO_2, and NADH. Two other dehydrogenase complexes, the 2-oxoglutarate dehydrogenase (OGDH) and branched-chain ketoacid dehydrogenase (BCKDH) complexes, share several structural and enzymatic properties with PDH, and catalyze an analogous reaction, by which a 2-oxoacid is oxidatively decarboxylated [2]. The three complexes are referred to collectively as DH complexes.

All three complexes, PDH, OGDH, and BCKDH, consist of three

* Corresponding authors.
E-mail addresses: jula@paru.cas.cz (J. Lukeš), skodovaister@gmail.com (I. Škodová-Sveráková).
[1] These authors contributed equally to this work.

https://doi.org/10.1016/j.bbagen.2023.130419
Received 2 February 2023; Received in revised form 27 June 2023; Accepted 28 June 2023
Available online 13 July 2023

distinct subunits referred to as the Enzyme 1, 2, and 3 (E1, E2, and E3), each having a particular catalytic function. The E1 subunit is a thiamine diphosphate-dependent enzyme with a 2-oxoacid dehydrogenase activity (also known as pyruvate, 2-oxoglutarate or ketoacid dehydrogenase) that catalyzes in a two-step reaction the irreversible decarboxylation of the substrate, and the reductive acylation of lipoyl groups covalently attached to E2. The E2 subunit, a dihydrolipoamide acyltransferase, catalyzes the transfer of an acyl moiety to CoA producing acyl-CoA. Finally, the E3 subunit, a flavoprotein with dihydrolipoamide dehydrogenase activity, transfers electrons from dihydrolipoyl groups of E2 to FAD and then to NAD^+ generating NADH + H^+ [3]. This E3 subunit is a member of the disulfide oxidoreductases family [4], which also includes glutathione reductase [5], thioredoxin reductase [6], trypanothione reductase [7], and mercuric reductase [8]. In eukaryotes, E3-binding protein (E3BP; also called Protein X) is a non-catalytic auxiliary protein of the PDH complex. This protein is structurally and functionally related to the E2 component and anchors E2 in the complex [9].

Across the tree of life, the **E1 subunit** of PDH typically consists of either a single polypeptide encoded by an *aceE* gene, as *e.g.*, in Gram-negative bacteria, or alternatively, as encountered in eukaryotes and Gram-positive bacteria [10], of a heterotetramer composed of two proteins, 2xE1-α and 2xE1-β, encoded by *pdhA* and *pdhB* genes, respectively [11,12]. (Note that for simplicity, we follow the gene nomenclature used in bacteria.) While functionally equivalent, the E1 components of the PDH, OGDH, and BCKDH complexes can have a different composition and the homologous proteins differ in sequence. For clarity, the homologs in the various complexes will be referred to in the following as E1p-α, E1o-α, and E1b-α, *etc.*

The **E2 subunit** consists of a single protein encoded by *aceF* (also designated *pdhC*) and forms the core of the PDH complex, physically interacting with both the E1 and E3 subunits [13]. Again, the E2 proteins from the three DH complexes differ in sequence and will be referred to as E2p, E2o, and E2b. Lastly, the homodimeric **E3 subunit** comprises two identical polypeptide chains, designated the 'E3 proteins' (encoded by *lpdA/pdhD*). In contrast to E1 and E2, the nature and distribution of the E3 subunit can be more complicated, depending on the organism: in some cases, the PDH, OGDH, and BCKDH complex each contains a DH-specific E3 [14], in others, all three DH complexes contain an identical E3 [15], while still in others, DH complexes are composed of E3 isoenzymes in various ratios [16].

Several exceptions to the conventional DH-complex structures exist. For example, Actinobacteria harbor an enzyme that carries out both E1 and E2 activities of the OGDH [17,18]. Moreover, the PDH and OGDH complexes are present in a mixed supercomplex [19]. Due to their functional similarity [20], mutual substitution of DH complexes occasionally occurs. For instance, in several apicomplexan parasites, BCKDH has taken over the function of PDH [21,22]. Furthermore, apicomplexan OGDH is capable of *in vitro* decarboxylating both pyruvate and branched-chain ketoacids, yet with a lower preference for pyruvate [23]. In addition to the canonical DH complexes, a 2-oxoadipate complex exist that is involved in the final degradation of lysine, hydroxylysine, and tryptophan. Notably, this complex contains E2o instead of a specific E2; hence, a cross-talk between the 2-oxoadipate and OGDH complexes was suggested [24].

We recently examined the gene complement involved in basic metabolic pathways in diplonemids, an abundant, ecologically important group of marine protists [25]. It appeared that diplonemids including the well-studied representative *Paradiplonema papillatum* (originally designated *Diplonema papillatum* [26]) are lacking the genes encoding subunits of the PDH complex. To identify the subunit composition of all DH complexes in diplonemids, we mined the genome of *P. papillatum*, and the transcriptomes of ten other diplonemids, for the expected DH subunits and compared them to those present in other euglenozoans [27]. In *P. papillatum,* we also determined the subcellular localization of the candidate proteins by shotgun proteomics and measured the enzymatic activities. Lastly, we used the functional genetics approach recently established for *P. papillatum* [28] for epitope-tagging of two putative DH subunits and pull down of their interacting partners. The obtained results allowed us to propose a scenario for the evolution of the three DH complexes in diplonemids and euglenozoans as a whole.

2. Materials and methods

2.1. Sequence searches and phylogenetic analyses

Subunits of *Trypanosoma brucei* [29] and *Euglena gracilis* [30] dehydrogenase complexes were used as queries in BLAST+ v2.8.1 [31] searches against the genome of *Paradiplonema papillatum* [32], transcriptomes of diplonemids *Diplonema japonicum*, *Diplonema ambulator*, *Rhynchopus humris*, *Rhynchopus euleeides*, *Lacrimia lanifica*, *Sulcionema specki*, *Flectonema neradi*, *Artemidia motanka*, *Hemistasia phaeocysticola*, and *Namystynia karyoxenos* [33,34] and euglenids *Euglena longa* [35] and *Eutreptiella gymnastica* ([36]; reassembly available at https://doi.org/10.5281/zenodo.257410), single-cell amplified transcriptomes of euglenids [37] and single-cell amplified genomes of euglenozoans [38]. For more sensitive searches, HMMER v3.3 [39] was employed. Protein domains were predicted using InterProScan [40] implemented in Geneious Prime v2020.2.5 [41]. Subcellular targeting was predicted by MitoprotII [42], MitoFates [43], and TargetP2 [44] in default settings.

Euglenozoan protein sequences were used in blastp searches against the NCBI non-redundant database to identify homologs from the main eukaryotic groups [45] and prokaryotes. Retrieved hits were used to build multiple sequence alignments using MAFFT v.7458 under L-INS-i strategy [46]. Poorly aligned positions were removed by trimAl v1.4 (−gt 0.8) [47] and sequences shorter than 50% of the length of the trimmed alignment were removed by an in-house python script (https://github.com/kikinocka/ngs/blob/master/py_scripts/filter_alignment.py). Resulting alignments were subjected to maximum-likelihood phylogenetic analyses by IQ-TREE v1.6.12 [48] under the LG+I+G4 (E1α, E1β, and E3) and LG+F+I+G4 (E2) models, which were determined as best-fitting according to Bayesian information criterion, and under the LG+C20+F+G model (AceE) using posterior mean site frequency method [49] with the guide tree inferred under the LG+F+G model. Branch supports were obtained by the ultrafast approximation [50] with 1000 replicates.

2.2. Gene tagging

We attempted to create an *in situ* C-terminally-tagged version of the E3 enzyme of *P. papillatum* (DIPPA_01402), but no stable, viable clones could be produced. Hence, the E3-Protein A fusion was ectopically expressed after random integration into the genome. The open reading frame (ORF) of DIPPA_01402 was amplified from *P. papillatum* genomic DNA using primers E3_Fw and E3_Rv and cloned into pDP002 vector [28] using *Bgl*II/BamHI and *Nhe*I restriction sites. The entire 5′UTR-E3-protein A-Neo^R-3′UTR cassette was amplified from the resulting plasmid using primers pDP002_cassette_Fw and pDP002_cassette_Rv, purified, and used for transfecting *P. papillatum*. To endogenously tag AceE (DIPPA_31725) with a C-terminal Protein A-tag, parts of the ORF (AceE_ORF_Fw and AceE_ORF_Rv) and UTR (AceE_3UTR_Fw and AceE_3UTR_Rv) were amplified from *P. papillatum* genomic DNA using primers containing sequences overlapping with the Protein A-Neo^R cassette of pDP002 [51]. Another PCR was done to amplify the protein A-Neo^R cassette from pDP002 [51] using primers Fw_protein A-Neo_cassette and Rv_protein A-Neo_cassette. To ligate of all three fragments together, they were used as templates in a nested PCR approach using primers AceE_nested_Fw and AceE_nested_Rv and Phusion polymerase (NEB) and the resulting product was A-tailed and cloned into pcr® 2.1-TOPO® (ThermoFisher). About 10 μg of the resulting plasmid was cut with *Eco*RI, ethanol precipitated, resuspended in 10 μl of water and used for transfecting *P. papillatum*. Primer sequences are listed in Table S1.

2.3. Strain, cultivation, and electroporation of P. papillatum

Paradiplonema papillatum (ATCC 50162; recently renamed from *Diplonema papillatum* [26]) was cultivated axenically in 36 g/l sea salt, 1 g/l tryptone and 1% (*v/v*) fetal bovine serum as described previously [51]. About 5×10^7 cells were transfected using an Amaxa Nucleofector II as described earlier [28,51]. The transfectants were selected at different concentrations of G418 (25 to 80 μg/ml) in 24-well plates at 27 °C. After two weeks, successful transfectants could be observed. Each clone was transferred to 20 ml medium and was cultured for 3–4 weeks prior to testing the expression of the tagged protein by immunoblotting.

2.4. Immunofluorescence assay

Roughly 20–30 ml of an exponential phase culture was centrifuged at 1000*g* for 5 min. Cells were resuspended in 500 μl of 4% paraformaldehyde (dissolved in sea water) and fixed for 20 min on Superfrost plus slides (Thermo Scientific, J1800AMNZ) at room temperature. The fixative was washed out from cells with 1× PBS. For antibody staining, cells were permeabilized in ice-cold methanol for 20 min. The slides were kept in a humid chamber throughout the procedure. Afterwards, the slides were washed with 1× PBS, and blocked for 45 min in 5.5% (*w/v*) fetal bovine serum in PBS-T (0.05% (*v/v*) Tween in 1× PBS). The blocking solution was removed, and cells were washed with 1× PBS. The rabbit anti-Protein A primary antibody (1:2000; Sigma, P3775) diluted in 3% (w/v) BSA (Bovine serum albumin, Sigma, A4503) in PBS-T was added on slides and incubated either for 2 h at room temperature or at 4 °C overnight covered with parafilm. Next, the primary antibody was removed, and slides were washed three times with PBS-T and twice with 1× PBS. AlexaFluor555-labeled goat anti-rabbit secondary antibody (1:1000; Invitrogen, A32732) was added and incubated at room temperature for 1 h in the dark, covered with parafilm. All slides were then rinsed three times with PBS-T and twice with 1× PBS and coated with 4′,6-diamidino-2-phenylindole (DAPI) containing the antifade reagent ProlongGold (Life Technologies). Images were acquired using an Olympus BX63 automated fluorescence microscope equipped with an Olympus DP74 digital camera and evaluated with the cellSens Dimension software (Olympus). Since MitoTracker Red and MitoTracker Green do not stain *P. papillatum* mitochondria (our observations), we employed rabbit antibody against β chain of mitochondrial ATP synthase (1: 200, kindly provided by Alena Zíková's laboratory; [52]) to visualize the organelle. Because both anti-ATP synthase β and anti-Protein A antibodies are of rabbit origin, simultaneous imaging of the same slide was not possible.

2.5. Immunoprecipitation

Rapid single-step purification of Protein A and its conjugates was used for tagged AceE and E3 protein purification. Two different cell lysates were prepared with two non-ionic detergents: 0.1% (*v/v*) IGEPAL CA-630 and 2% (*w/v*) dodecyl maltoside (DDM). Approximately 5×10^8 cells expressing Protein A-tagged E3, as well as wild-type control cells were grown axenically in vented flasks at 27 °C in seawater-based tryptone-rich medium (36 g/l sea salt, 1 g/l tryptone and 1% (*v/v*) fetal bovine serum) with the appropriate selection antibiotic G418 (75 μg/ml). Cells were harvested by centrifugation at 1000*g* for 10 min. After that, cells were resuspended in 5 ml of ice cold 1× PBS, centrifuged again at 1000*g* for 10 min, and the supernatant was discarded. The pellet was resuspended in ice cold 1× PBS and irradiated with 600 mJ/cm2 UV light (254 nm wavelength) to covalently crosslink proteins (UV Stratalink 1800, Stratagene). UV-crosslinked cells were lysed using lysis buffer (10 mM Tris (pH 6.8), 150 mM NaCl, 0.1% IGEPAL CA-630, 1% (*v/v*) glycerol, 1× cOmplete EDTA-free protease inhibitors; Roche) and passed through a 30-gauge needle several times. The cell lysate was cleared twice by centrifugation at 10,000*g* for 20 min. 75 μl IgG Sepharose 6 Fast Flow beads (Sigma) were added to the cleared cell lysate and rotated at 4 °C for 2 to 3 h. The beads were washed three times with the washing buffer (10 mM Tris (pH 6.8), 250 mM NaCl, 1% (*v/v*) glycerol) supplemented with 0.1% (*v/v*) IGEPAL CA-630, and then twice with the washing buffer without the detergent. Bound proteins were eluted from the beads with 100 μl of 0.1 M glycine (pH 3.0) by rotating for 5 min at room temperature and immediately mixed with 10 μl of 1 M Tris-HCl (pH 9.0). Small aliquots of input, flow through, and elution fraction were used for immunoblotting. The elution fraction was subsequently sent for mass spectrometry analysis. The same procedure was performed for Protein A-tagged AceE, except for crosslinking. DDM lysates were processed similarly, except for the crosslinking step and rotation.

2.6. Subcellular fractionation

Cultivation and fractionation were performed essentially as described earlier [53]. Briefly, cells were cultivated axenically without shaking at ~20 °C in ocean salt medium containing 33 g/l Instant Ocean Sea Salt (Instant Ocean) supplemented with 1% (*v/v*) horse serum (Wisent) and 0.04% (*w/v*) yeast extract (BioBasic). Cells were grown until the late exponential phase, harvested by centrifugation (2000*g*, 4 °C, 5 min), resuspended in a buffer containing 1.2 M sorbitol, 20 mM HEPES pH 7.5, 2 mM EDTA pH 8.0, and 1× cOmplete EDTA-free protease inhibitors (Roche), and then lysed in a nitrogen cavitation chamber (Parr Instrument Company) under 30-bar nitrogen pressure. The cell lysate was separated by ultracentrifugation on a two-step sucrose gradient (36% and 60%; 134,000*g*, 4 °C, 60 min). The top fraction (above 36% sucrose) corresponded to the cytosol, while the fraction enriched in mitochondria was collected from the 36/60% sucrose interface. A detailed protocol is available at 10.17504/protocols.io.pkydkxw.

2.7. Mass spectrometry and data analysis of immunoprecipitated samples

Trypsin digestion of the eluted Protein A-tagged E3 and wildtype control samples was performed prior to liquid chromatography-tandem mass spectroscopy (LC-MS/MS) as previously described [54]. Data were processed using MaxQuant v1.6.14 [55], which incorporates the Andromeda search engine [56]. Proteins were identified by searching a custom protein sequence database of *P. papillatum* (43,871 sequences) supplemented with frequently observed contaminants. Default search parameters were employed by MaxQuant for Orbitrap analyzers with full trypsin specificity, allowing for up to two missed cleavages. Carbamidomethylation of cysteine was set as a fixed modification and oxidation of methionine and N-terminal protein acetylation were allowed as variable modifications. The experimental design included matching between runs for biological replicates. Peptides were required to be at least seven amino acids long, with false discovery rates (FDRs) of 0.01 calculated at the levels of peptides, proteins, and modification sites based on the number of hits against the reversed sequence database. Protein quantification was done using iBAQ indices (raw intensities divided by the number of theoretical peptides) allowing comparison of protein abundances both within samples and between them. After filtering to remove any protein with less than two unique peptides and an Andromeda score of <20, the obtained data were processed in Perseus v1.6.14 as described previously [57].

2.8. Proteomic analysis of subcellular fractions

Proteomic analysis of *P. papillatum* subcellular fractions was performed as described earlier [58]. Briefly, aliquots of 50 μg of purified mitochondria, cytosol, and cells were lysed with 6 M urea in 50 mM triethylammonium bicarbonate pH 8 (both Sigma-Aldrich). Subsequently, four biological replicates of each sample were reduced, alkylated, and digested with trypsin (Promega; 1:50 enzyme to protein ratio). Peptides were purified on custom-made microtips with

LiChroprep RP-18 25–40-μm particles (Merck-Millipore). Next, their concentration was measured by the Pierce quantitative fluorometric peptide assay (Thermo Fisher Scientific).

For liquid chromatography-coupled mass spectrometry, peptides were loaded onto a trap column (PepMap100 C18, 300 μm × 5 mm, 5-μm particle size; Dionex) and separated with an EASY-Spray C18 analytical column (75 μm × 500 mm, 5-μm particle size; Thermo Fisher Scientific) on Ultimate 3000 RSLCnano system (Dionex). The gradient of 2.4–34.4% acetonitrile was applied for 2 h at a flow rate 250 nl/min. Spectra were collected by Orbitrap Elite (Thermo Fisher Scientific) in the data-dependent Top15 mode. Precursors were measured in the mass range 300–1700 *m/z* with a resolution 120,000, fragmented by the HCD mechanism with normalized collision energy 25 and acquired at a resolution 15,000.

Datasets were processed by MaxQuant v1.6.17.0 using the Andromeda search engine as described in the previous section; however, precursor tolerance in the first search was set to 20 ppm, and 4.5 ppm in the main search upon recalibration, fragment tolerance was 20 ppm, and N-terminal protein acetylation was disallowed. The label-free quantification of proteins relied on LFQ intensities (essentially the sum of peptide intensities normalized for median peptide ratios between samples).

The statistical analysis was performed using Perseus v1.6.15.0. The Output proteinGroup table from MaxQuant was filtered and LFQ intensities $\log_2$-transformed. Proteins with less than one missing value in at least one experimental group were retained and data imputed, assuming a normal distribution. The principal component analysis confirmed excellent analytical reproducibility and ANOVA corrected by permutation test was used with a $Q \leq 0.001$. Pairwise differences were assessed by the Tukey's test with $P \leq 0.001$. Hierarchical clustering was performed on *Z*-score-normalized averages of LFQ intensities.

To quantitatively compare DH complex components relative to each other, LFQ intensities were normalized to the number of theoretically detectable peptides, *i.e.*, as in the iBAQ approach [59]. The number of trypsin peptides for each DH complex protein was determined using the MS-Digest tool from the ProteinProspector v6.3.1 tool suite (http://prospector.ucsf.edu/prospector/cgi-bin/msform.cgi?form=msdigest). We used the following parameters: trypsin digest; no missed cleavage; carbamidomethyl at Cys residues as fixed modification; Met oxidation as a variable modification; minimal length of 7 amino acids; and peptide mass range from 900 to 5000 Da; the selected mass range covered >95% of all identified peptides.

2.9. Immunoblotting

Protein samples obtained from immunoprecipitation were boiled for 5 min in 2× NuPAGE LDS sample buffer (Invitrogen), run on 12% SDS-PAGE, and transferred to a PVDF membrane (Amersham). After blocking with 5% (*w/v*) milk in PBS-T (0.05% (*v/v*) Tween in PBS) for at least 30 min at room temperature, the membrane was incubated with rabbit anti-Protein A primary antibody (1:10,000; Sigma-Aldrich, P3775) at 4 °C overnight. After three washes in PBS-T, the membrane was incubated with HRP-coupled goat anti-rabbit secondary antibody (1:1000; Sigma-Aldrich, A21428) at room temperature for 1 h. The membrane was then washed three times in PBS-T, and the signal was developed using Clarity Western ECL Substrate (Bio-Rad). An analogous procedure was used to test the expression of tagged proteins in whole cells. The mouse anti-α-tubulin antibody (1:10,000; Sigma-Aldrich, T9026) was used as a loading control.

The effect of the Protein A-tag on the integrity of DH complexes was monitored by their separation using Clear-Native (CN) PAGE followed by immunoblotting. Briefly, mitochondria were isolated using solubilization by DDM as described previously [60], and 120 μg of total mitochondrial proteins was loaded into each well. Half of the gel was stained with Coomassie Brilliant Blue G-250 (CBB) to control for equal protein loading. The other half was transferred onto a nitrocellulose membrane overnight at 20 mA. Immunodetection with rabbit anti-Protein A primary antibody was performed as described above.

2.10. Activity measurements

Aliquots of 100 μg of mitochondrial proteins were used to assess the PDH and OGDH activity. The wild-type (WT) *P. papillatum* ATCC 50162 (or its genetically altered derivate) was grown axenically in vented flasks at 15 °C in seawater-based tryptone-rich medium (36 g/l sea salt, 1 g/l tryptone and 1% (*v/v*) fetal bovine serum) or tryptone-poor medium (36 g/l sea salt, 0.01 g/l tryptone, and 1% (*v/v*) horse serum). The pyruvate dehydrogenase activity was determined using a commercial kit (Sigma-Aldrich, MAK103) for coupled enzymatic reaction, which resulted in a colorimetric (450 nm) product proportional to the enzymatic activity.

The OGDH activity was monitored in 1 ml assay buffer (50 mM Kpi pH 7.4; 2 mM $MgSO_4$; 6 mM NAD^+; 2 mM thiamine pyrophosphate; 4 mM CoA). The reaction was started by addition of 2-oxoglutarate in 20 mM concentration. Increase in NADH was monitored at 340 nm for 5 min. One unit of activity (U) is the amount of enzyme that generates 1 nmol of NADH per minute.

The BCKDH activity was tested in various conditions as reported in published protocols [61–63]; however, none of these conditions worked in the protist.

3. Results

3.1. Predicted composition of dehydrogenase complexes in diplonemids

To identify the components of the DH complexes in diplonemids, we searched in the genome- and transcriptome-inferred proteomes of 11 species (*P. papillatum*, *D. japonicum*, *D. ambulator*, *R. humris*, *R. euleeides*, *L. lanifica*, *S. specki*, *F. neradi*, *A. motanka*, *H. phaeocysticola*, and *N. karyoxenos*) for homologs of proteins constituting the DH subunits previously described in *T. brucei* [29] and *E. gracilis* [30]. From each diplonemid species, we retrieved eight distinct E1-subunit proteins, two E2-proteins, and a single E3 protein (Table S2).

To determine the affiliation of these proteins to a particular DH complex, we performed phylogenetic analyses including sequences from organisms spanning the diversity of eukaryotes and prokaryotes (Fig. 1; Fig. S1). The phylogenetic analyses clearly distinguished clades of subunits specific for different DH complexes. All diplonemids examined appear to encode a single E3 (represented by the *P. papillatum* protein DIPPA_01402), while the other euglenozoans have several homologs of this subunit. The diplonemid E3 groups with its E3 counterparts known to be shared by OGDH and BCKDH in its closest relatives, kinetoplastids and euglenids. For E2, we found one homolog each of the OGDH- and BCKDH-specific proteins (represented in *P. papillatum* by DIPPA_17068 (E2o) and DIPPA_02535 (E2b), respectively); however, we could not identify an E2 specific for PDH (E2p). Phylogenetic analyses of E1α and E1β indicates that DIPPA_25191 and DIPPA_04229 are components of the OGDH complex, while DIPPA_70163 and DIPPA_14886 belong to the BCKDH complex. An additional homolog (DIPPA_08195) that did not cluster with any of the assigned DH complexes possibly belongs to another unknown DH complex referred to here as 'unspecified' DH. None of the diplonemid E1 sequences grouped with the PDH (E1p) sequences from other eukaryotes. Instead, we found two orthologs of prokaryotic AceE proteins. One (DIPPA_31725) is related to archaeal *AceE* and is present in all examined diplonemids. The second ortholog, which groups with the bacterial counterpart, is confined to a subgroup of Hemistasiidae (Fig. 1; Fig. S1).

Active regions and residues of E2o were previously identified in the catalytic domain of the *E. coli* protein [64], which allowed us to investigate their counterparts in the euglenozoans. We separately aligned euglenozoan E2 sequences from different phylogenetic clades with the *E. coli* sequence (Fig. S2). The corresponding regions of E2o possess the highest percentage of pairwise identity of all three regions. Moreover,

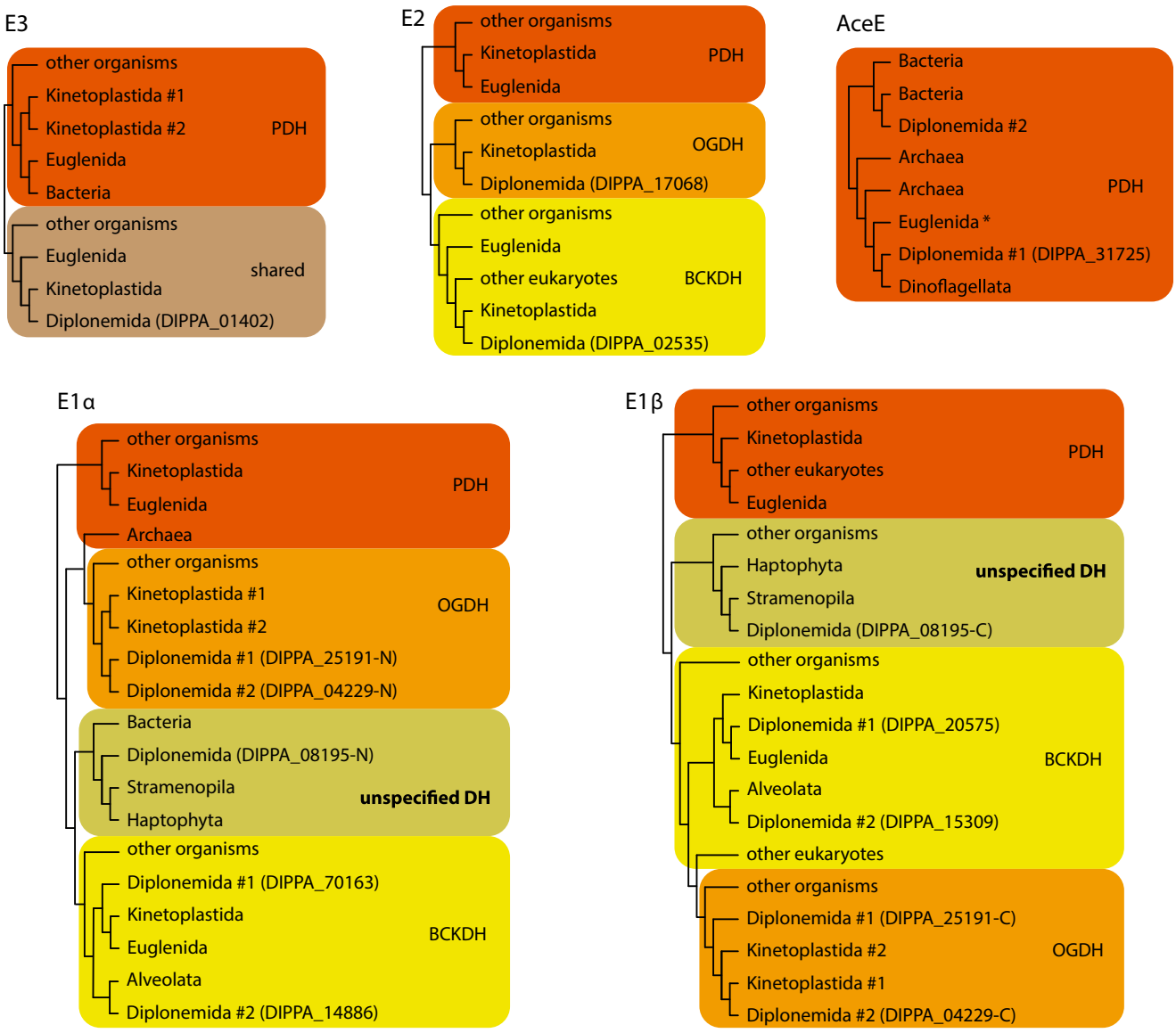

Fig. 1. Schematic phylogenetic trees of subunits of dehydrogenase complex subunits. Each tree represents a summary version of the full tree shown in Fig. S1. All presented branches were supported by >90% ultrafast bootstraps (except for the E2b kinetoplastid/diplonemid split at 45%). Euglenozoan taxa are in bold. The identifier of *Paradiplonema papillatum* proteins representing Diplonemida is indicated in parentheses. Paralogous sequences are labeled '#1' and '#2'. To analyze E1 subunit sequences irrespective of their existence as a single chain or two polypeptides, we split, prior to the construction of multiple sequence alignments, single polypeptides into their 'N' and 'C' moieties that correspond to the E1α and E1β subunits, respectively (indicated by these suffixes for the *P. papillatum* IDs). The asterisk indicates partial sequences from two *Anisonema* strains, whose eukaryotic origin remains to be confirmed by full genome or transcriptome sequencing.

two out of three *E. coli* residues responsible for the E2o's substrate specificity [64] are conserved only in the phylogenetically assigned E2o sequences from euglenozoans (Fig. S2). Collectively, these results support the protein classification obtained by our phylogenetic analyses. We also investigated the distribution of lipoyl-binding domains, the number of which was previously proposed to correlate with the DH complex type [20]. However, we found no informative correlation among the euglenozoan sequences (Table S3), suggesting that the previous conclusion [20] might have been biased by a limited sampling across the diversity of organisms available at that time.

Based on the phylogenetic analyses, we inferred the following makeup of E1 subunits across the three DH complexes from euglenozoans. In kinetoplastids and euglenids, the E1p subunit consists of two proteins, E1p-α and E1p-β, but of a single protein, an AceE homolog, in diplonemids. E1o from kinetoplastids and diplonemids is a single fusion protein composed of the E1-α and β proteins (E1o-α+β), whereas this subunit is absent from euglenids. The situation of the E1b subunit is simpler, as it consists in all euglenozoans of an α and β protein (Fig. 2). Further, the examined diplonemids encode an additional E1-α+β fusion, but the DH complex it belongs to has yet to be identified.

We have identified in several kinetoplastid and euglenid flagellates orthologs of the non-catalytic E3BP previously described in *T. brucei* [29] (Table S4). Importantly, no E3BP homolog was found in any diplonemid species, even when more sensitive searches with a euglenozoan-specific profile hidden Markov model was employed. Altogether, our results strongly suggest that the canonical PDH complex was lost from the diplonemid lineage.

3.2. Mitochondrial localization of dehydrogenase complexes in *P. papillatum*

To determine the ratios of the 11 postulated components of the three DH complexes, and to verify the predicted mitochondrial localization (Table S2) of the corresponding proteins, we conducted liquid

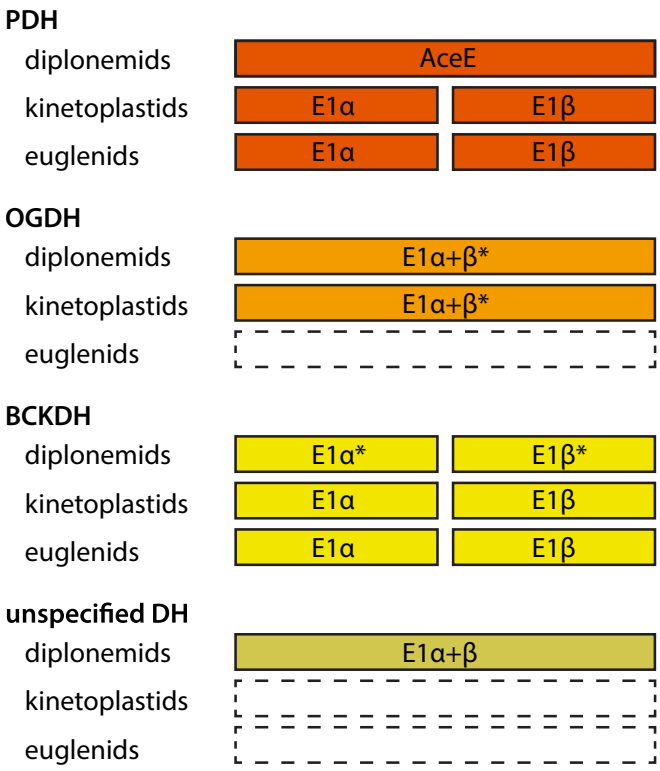

Fig. 2. The structure of E1 subunit genes in euglenozoans. Asterisks indicate the presence of two paralogs. The structure of euglenid E1p is based on that of the model *Euglena gracilis*, however, AceE was identified in *Anisomena acinus* (Fig. S1A).

chromatography-tandem mass spectrometry (MS) of whole-cell lysates and subcellular fractions enriched in either cytosolic or mitochondrial proteins (Fig. 3; Table S5A).

Principal component analysis of the MS experiments showed satisfactory distinctiveness and reproducibility (Table S5B). For instance, the cytosolic fraction was enriched in cytosolic ribosomal proteins and translation factors, proteasome subunits, as well as metabolic enzymes involved in glycolysis and gluconeogenesis, while the mitochondrial fraction contained typical organellar proteins, such as respiratory chain complex components, carrier proteins, and prohibitins (Table S5C). All above identified subunits of the *P. papillatum* DH complexes were significantly enriched in the mitochondrial fraction, except for the inferred protein DIPPA_15309 (E1b-β #2), which was not detected in any sample (Fig. 3), even though the gene is transcribed at a level similar to that of other subunits (Table S2).

To further validate experimentally the mitochondrial localization of DH complexes, we created *P. papillatum* cell lines expressing DIPPA_31725 (AceE) and DIPPA_01402 (E3) that were C-terminally tagged with Protein A (Fig. S3). C-terminal tagging was chosen to avoid interference with mitochondrial import signals generally located at the N-terminus. The resident AceE gene was replaced by the tagged version. However, in the case of E3, knock-in did not succeed, so that we introduced an ectopic copy of the tagged E3 gene into the genome. Immunofluorescence-based detection with anti-Protein A antibodies showed that AceE and E3 localized to the single reticulated mitochondrion (Fig. 4). As a control, the mitochondrion was immunolabeled with an antibody against the β chain of the mitochondrial ATP synthase. The staining pattern observed using the anti-ATP synthase antibody strongly resembled the signals obtained with AceE and E3, confirming the predicted mitochondrial localization of these two DH-complex components.

3.3. Purification of DH complexes from P. papillatum

To evaluate whether the Protein A-tagged subunits E3 and AceE

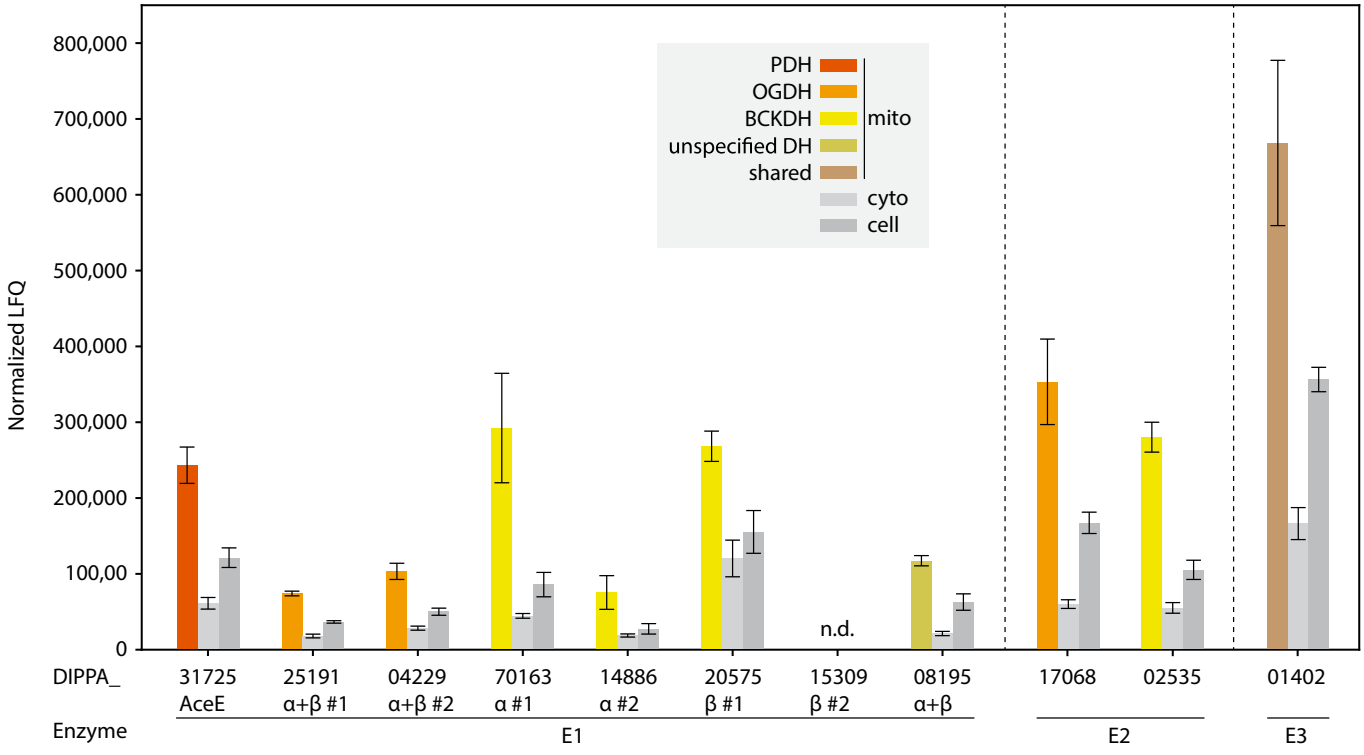

Fig. 3. Subunit enrichment of dehydrogenase complexes in cellular fractions of *P. papillatum*. The assignment of subunits to DH complexes was based on phylogenetic analyses. The label-free quantification of proteins was based on label-free quantitation (LFQ) intensities (see also Table S5). PDH, pyruvate dehydrogenase complex; OGDH, 2-oxoglutarate dehydrogenase complex; BCKDH, branched-chain ketoacid dehydrogenase complex; n.d., not determined.

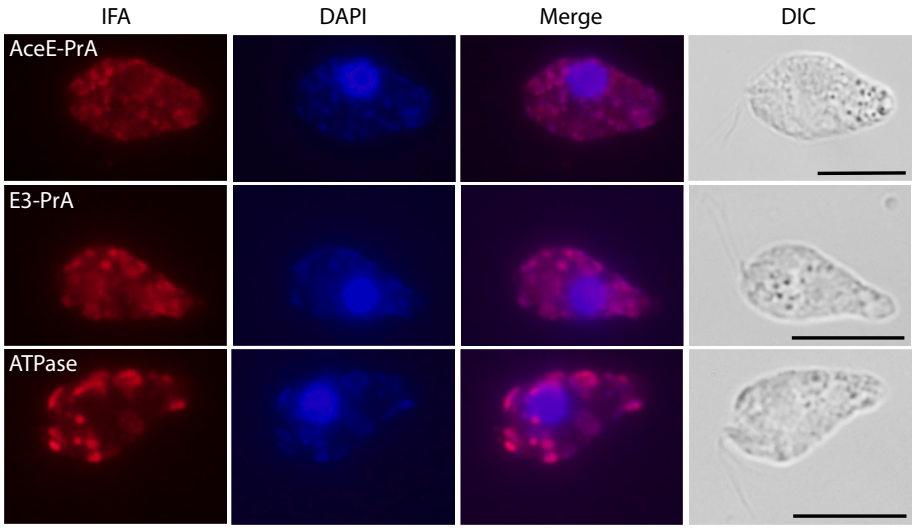

Fig. 4. Subcellular localization of AceE and E3 proteins in *P. papillatum*. Immunofluorescence assay (IFA) of Protein A-tagged AceE (first row) and E3 (second row) proteins using polyclonal anti-Protein A antibodies (red) confirmed their mitochondrial localization. Rabbit-antibodies against mitochondrial ATP synthase (third row) were used for comparison (see Methods). DNA was stained with DAPI (blue). The scale bar is 10 μm. DIC, differential interference contrast. (For interpretation of the references to colour in this figure legend, the reader is referred to the web version of this article.)

assembled into large complexes, we extracted mitochondrial proteins, separated them *via* CN-PAGE (2–10% gradient gel), and performed immunoblotting. We observed signals at a high molecular weight (upper area of the gel; Fig. 5), which indicated the incorporation of the tagged proteins into complexes. However, the vast majority of the Protein A-tagged AceE was detected as a smear of varied molecular weights centered around 600 kDa, which suggested disassembly and/or degradation of a much larger (presumably PDH) complex during protein extraction. The Protein A-tagged E3 displayed a less prominent smear of apparent disassembly products but was also detected as a distinct signal in the low molecular-weight region (presumably as a monomer) (Fig. 5).

To investigate the composition, the three DH complexes from *P. papillatum* were pulled down using the C-terminally-tagged AceE and E3 proteins and analyzed by MS. We reasoned that if the E3 protein was part of all three DH complexes, it would pull down all complexes, whereas AceE, which we expected to be an exclusive component of the PDH complex, would only pull down this single complex. Immunoblotting of the fraction pulled down *via* the E3 protein confirmed that the eluate was enriched in the bait protein (Fig. 6). MS analysis of this fraction revealed three proteins strongly associated with the E3 protein, which were all predicted components of the OGDH complex, namely DIPPA_25191 (E1o-α+β #1), DIPPA_04229 (E1o-α+β #2), and DIPPA_17068 (E2o). E2b (DIPPA_02535) was also detected but at low abundance and below the significance threshold (Fig. 5), while subunits of the PDH complex were absent from the eluate. In a separate set of experiments, we immunoprecipitated the tagged AceE, but MS analysis did not uncover any interactors at significant amount and enrichment.

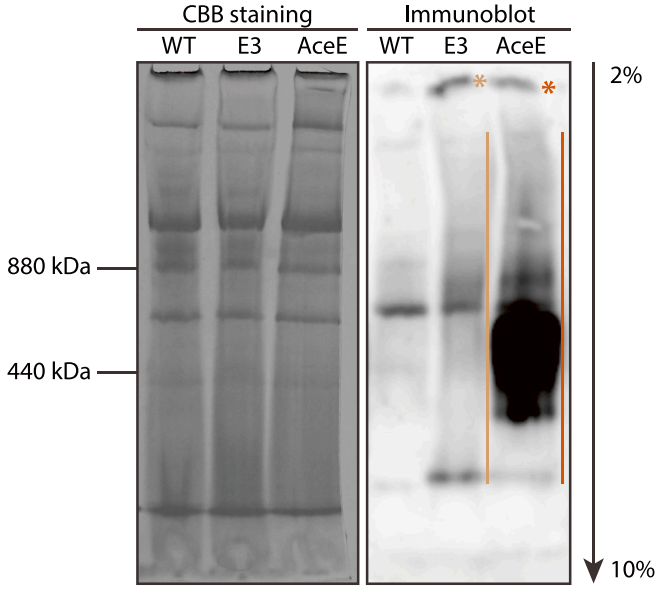

Fig. 5. Immunodetection of complexes *via* Protein A-tagged E3 and AceE on native gel. Coomassie brilliant blue (CBB) staining (left panel) served as a loading control. The right panel shows the immunoblotting of proteins using anti-Protein A antibodies. Asterisks indicate large complexes, while the signals in the lower molecular-weight region represent disassembly and/or degradation products and unspecific epitopes. (For interpretation of the references to colour in this figure legend, the reader is referred to the web version of this article.)

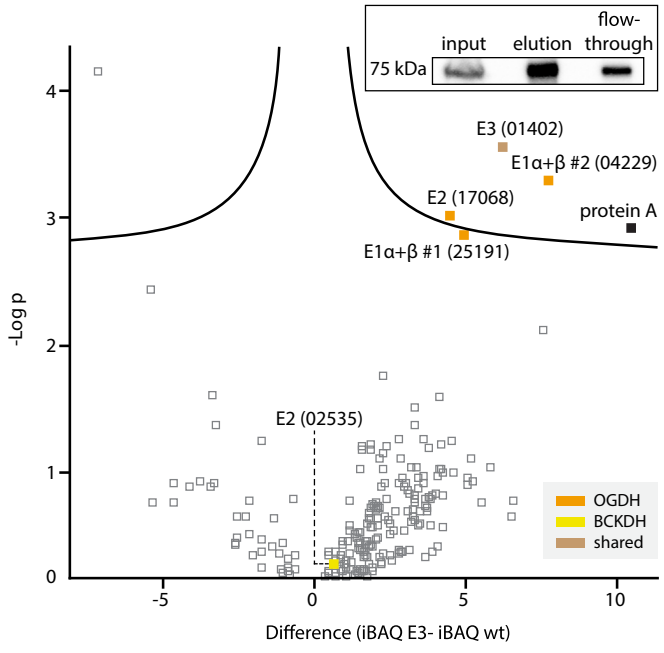

Fig. 6. Immunopurification of E3. Volcano plot of the $-\log_{10} p$ value of the *t*-test plotted against the intensity-based absolute quantification (iBAQ) difference between the samples of the Protein A-tagged E3 subunit and wildtype (wt) control, based on three biological replicates. Statistically significant hits are placed above the curve in the top right quadrant; their identity is indicated. Hits are colour-coded according to the complex they belong to. The inset shows an immunoblot of a representative immunoprecipitation; the blot was probed with anti-Protein A antibodies to detect tagged E3.

Essentially identical results were obtained when the detergent used for the pull-down experiments, octylphenoxypolyethoxyethanol (IGEPAL), was replaced by n-dodecyl-beta-D-maltoside (DDM) (for details, see Tables S6 and S7).

3.4. Activity measurements

To show that PDH and OGDH are indeed present in *P. papillatum*, we measured the activities of these complexes in mitochondria of the WT and tagged cell lines (Table 1). The presence of the tag did not inactivate either the PDH or the OGDH complex. Due to technical difficulties, we could not evaluate the effect of the Protein A-tagged E3 on the activity of the BCKDH complex.

4. Discussion

4.1. The E3 protein is likely a shared component of all three DH complexes in diplonemids

The PDH, OGDH, and BCKDH complexes share mechanistic and structural similarities but carry out distinct enzymatic reactions in the cell. While traditionally viewed as highly conserved across all domains of life, recent studies have shown that in some organisms a given subunit of one complex can mix with and substitute its homologous counterpart from another complex [15], leading to hybrid complexes [65]. The most widespread example of such an architectural plasticity is the E3 protein, which, in many bacteria (*e.g.*, *E. coli*) and eukaryotes (*e.g.*, land plants, animals, euglenozoans) is a constituent of two or even three different DH complexes [16,66].

Unexpectedly, the tagged E3 protein of *P. papillatum* pulled down exclusively the OGDH complex. From the BCKDH complex, we detected only insignificant traces, and from the PDH complex not a single protein. Still, several lines of evidence indicate that the E3 protein is not exclusively associated with the OGDH complex. First, in isolated mitochondria of *P. papillatum*, the E3 protein is almost twice as abundant as E2o (Fig. 3). Thus, the 'surplus' E3 could be part of the elusive PDH complex. This is corroborated by the fact that complexes have generally several times less copies of E3 than of E1 and E2. Still, in an individual DH complex, the ratio between the subunits E1, E2, and E3 can fluctuate *in vivo*, and the architecture and the size of the complexes vary among organisms [19,67,68]. In mammals and fungi, for example, individual PDH complexes have E1:E2:E3 ratios of ~30:60:6 and ~20:60:12, respectively [68,69]. The reason for this variability is unclear.

Second, our measurements of the pyruvate dehydrogenase activity from *P. papillatum* in isolated mitochondria suggests the presence of a PDH complex. However, we cannot exclude as discussed later that the BCKDH complex catalyzes pyruvate decarboxylation.

Third, our CN-PAGE separations indicated that E3 and AceE-containing complexes of *P. papillatum* are unstable. This might be an inherent feature of these complexes because it was shown that the PDH complex from human and yeast easily disintegrate during isolation [70,71]. Alternatively, the tags that we appended to the AceE and E3 proteins may have destabilized the complexes of which these proteins are part. Although tagged E3 seems to be readily assembled into the OGDH complex, the tag could obstruct E3 integration into the other two complexes. Detection of all BCKDH proteins (except for the second paralog of E1b-β) and the AceE homolog in the mitochondrial fraction strongly suggests that both the OGDH and BCKDH complexes correctly assemble in wild-type cell lines and do comprise E3, even though direct experimental evidence for the existence of these complexes is yet to be provided.

Table 1
Activity measurements of *Paradiplonema papillatum* mitochondrial lysates.[a]

	PDH [U/mg]	OGDH [U/mg]	BCKDH [U/mg]
WT	14.7 ± 5.6	3.3 ± 1.1	n.d.
E3	13.5 ± 5.0	5.2 ± 1.6	n.d.
AceE	10.5 ± 3.6	5.9 ± 0.7	n.d.

[a] One unit of activity (U) is the amount of enzyme that generates 1 nmol of NADH per minute. Activities were calculated from 2 to 3 biological replicates. n.d., not determined.

4.2. Structure of the hypothetical diplonemid PDH complex: The E2 subunit has likely been replaced

Our extensive sequence searches failed to retrieve an E2p homolog from any diplonemid genome or transcriptome, which suggests that in contrast to the vast majority of organisms, diplonemids genuinely lack a PDH-specific E2. We posit that E2p is substituted by E2 from either OGDH or BCKDH, a situation not without precedents. In humans, for instance, the E2o and E3o subunits associate not only with the E1o protein to form the typical OGDH, but also with the evolutionarily much younger E1a protein that is specific for the 2-oxoadipate DH complex [24]. Similarly, in the bacterium *Corynebacterium glutamicum*, the PDH and OGDH complexes have the same E2 and E3 subunits but distinct E1p and E1o subunits [65].

It is currently unclear whether the presumed PDH complex in diplonemids comprises E2o or E2b, but hints come from *in vitro* activity tests of the three DH complexes, as well as instances of complete loss of the PDH complex in certain organisms. First, the inability of purified mammalian PDH to oxidize 2-oxo-glutarate *in vitro* suggests that the high substrate specificity prevents this complex from substituting the activity of OGDH [71]. In contrast, BCKDH from *Bacillus subtilis* is capable to decarboxylate pyruvate (but not 2-oxoglutarate) *in vitro*, albeit with lower specificity and efficacy than branched-chain ketoacids [72]. Lastly, in the apicomplexans *Toxoplasma gondii* and *Plasmodium falciparum*, the absence of PDH is fully compensated for by BCKDH, but not OGDH [22]. All this suggests that the BCKDH complex is more permissive to utilize pyruvate as a substrate.

One possibility is that similarly to apicomplexans [22], it is the BCKDH complex that carries out the mitochondrial PDH activity in *P. papillatum*. However, this scenario is not very likely, because apicomplexans lack all proteins otherwise present in the PDH complex, whereas diplonemids possess a dedicated E1p in the form of AceE, strongly suggesting that a functional PDH complex is indeed present in the latter group. We consider the E2b of the BCKDH complex as the most promising E2p candidate of the PDH complex, because the former complex can facilitate the PDH activity [22]. But an investigation in which E2 subunit associates with the diplonemid PDH complex, requires experimental approaches that, in contrast to protein tagging, fully maintain the native complex structure. One possibility would be the less disruptive purification on AMP-Sepharose, which is, however, complicated by the high background of NAD^+-dependent dehydrogenases and ATP dependent kinases (our unpublished data).

4.3. Structure of the hypothetical diplonemid PDH complex: Recruitment of an alien E1p

Typically, the E1p subunit of eukaryotes is made up of E1p-α and E1p-β proteins [73]. The corresponding genes are encoded in the genomes of various euglenozoans [29,30] – except for diplonemids. Apparently the diplonemid E1p heterotetramer was replaced with a prokaryotic AceE protein. Although we failed to identify experimentally the protein partners interacting with AceE, we showed that its Protein A-tagged version assembles into high molecular-weight complexes, although these are very fragile under all tested isolation conditions. Importantly, the relatively high abundance of this component in mitochondria attests to its functional importance.

All diplonemids possess an AceE homolog, and we also discovered the gene in the single-cell transcriptomes of the euglenid *Anisonema*, but not in *E. gracilis* and *E. longa* (Fig. S1A). As euglenids other than *Euglena*

spp. are poorly represented in public sequence repositories, it is plausible that *Anisonema* is not an exception in this protist lineage. Still, it needs to be confirmed by genomic and/or transcriptomic data that the partial *Anisonema* AceE sequences do not represent a contamination. If truly of euglenid origin, we can envisage two scenarios. The *AceE* gene was i) acquired either early on by the last common ancestor of euglenozoans with the subsequent loss in the lineage leading to kinetoplastids and certain euglenid lineages; or ii) several times independently from a related sources by the last common ancestor of diplonemids and by an euglenid lineage. Taxonomically broader sampling will be necessary to solve this question.

The picture is further complicated by an AceE homolog present in essentially all examined dinoflagellates [11], a taxon unrelated to euglenozoans. Our phylogenetic analysis indicates that the ancestor of dinoflagellates acquired the archaeal type of *AceE via* horizontal gene transfer from an euglenozoan. Both groups are marine protists inhabiting the same oceanic depths (Aleš Horák, pers. commun.), making this scenario highly plausible. Curiously, dinoflagellates also appear to have lost the E2p subunit, but retained its E2o and E2b counterparts (Fig. S1D) [11]. Such a convergence of gene repertoire in unrelated lineages strongly suggests that the original E2p was incompatible with the newly acquired E1p substitute in the form of AceE and thus another E2 subunit filled in its role (Fig. 7).

Surveying the distribution of DH components across poorly studied Euglenozoa will likely shed light on whether the acquisition of *AceE* is invariably accompanied by the loss of E2p and replacement by E2o or E2b, as seen in diplonemids and dinoflagellates. Such studies also promise to provide insight into the prerequisites and consequences of integrating alien components into a critically important enzyme complex.

CRediT authorship contribution statement

Kristína Záhonová: Conceptualization, Methodology, Investigation, Writing – original draft, Visualization. **Matus Valach:** Methodology, Investigation, Writing – original draft, Visualization. **Pragya Tripathi:** Methodology, Investigation, Writing – review & editing. **Corinna Benz:** Methodology, Investigation, Writing – review & editing, Visualization.

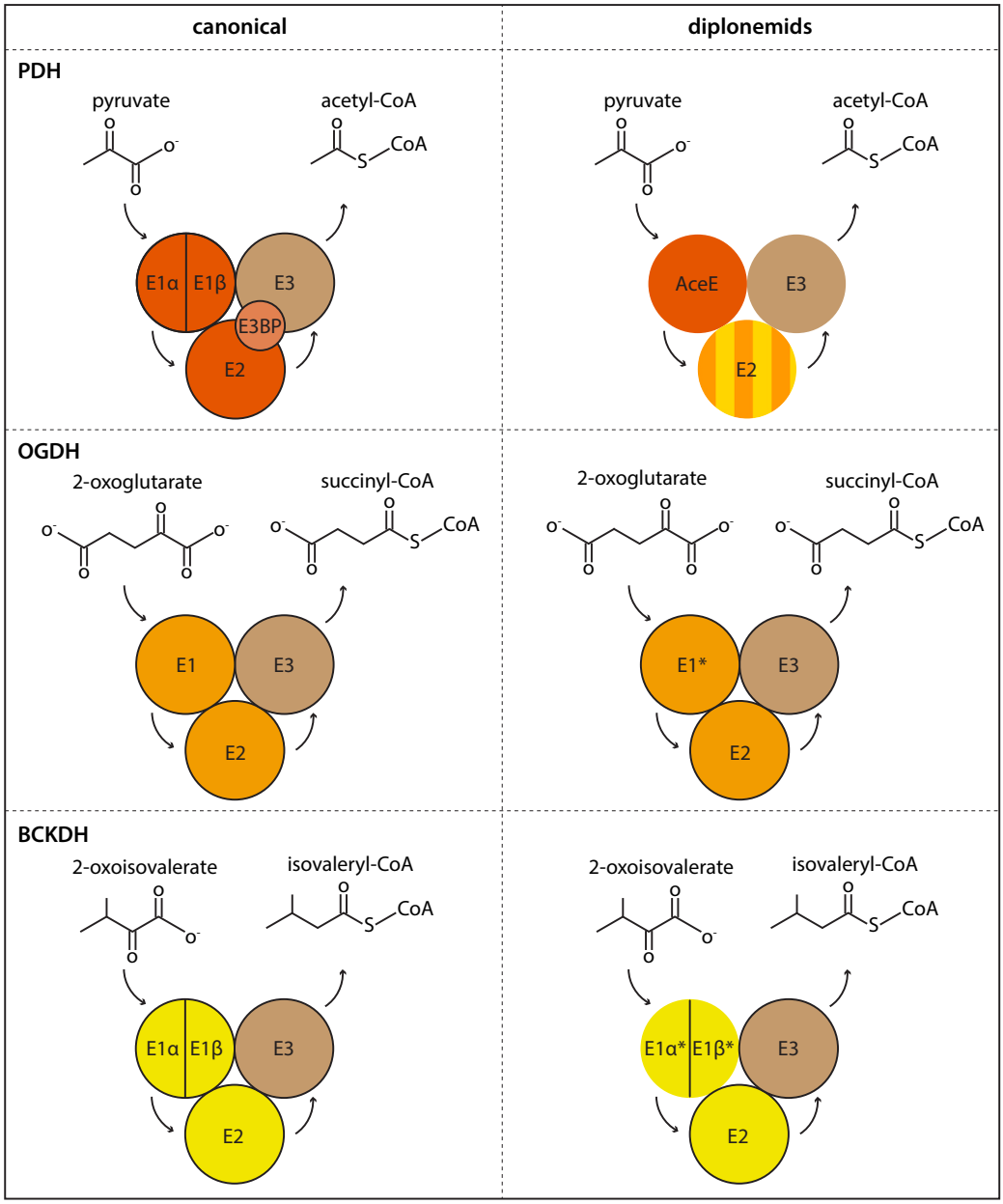

Fig. 7. Comparison of canonical and inferred diplonemid dehydrogenase complexes. A PDH-specific E2 subunit was not identified in diplonemids. We assume that it is functionally substituted by E2o and/or E2b. Subunits experimentally confirmed in *P. papillatum* are indicated by black borders. The scheme is only illustrative and does not reflect the subunit ratios found in the mitochondrion. The lighter shade of E3BP indicates that this subunit is present exclusively in eukaryotes, whereas other components are common to all organisms. Asterisks indicate that two paralogs are present. PDH, pyruvate dehydrogenase complex; E3BP, E3-binding protein; OGDH, 2-oxoglutarate dehydrogenase complex; BCKDH, branched-chain ketoacid dehydrogenase complex.

Fred R. Opperdoes: Conceptualization, Investigation, Writing – review & editing, Funding acquisition. **Peter Barath:** Methodology, Investigation, Writing – review & editing, Funding acquisition. **Veronika Lukáčová:** Methodology, Investigation, Writing – review & editing. **Maksym Danchenko:** Methodology, Investigation, Writing – review & editing. **Drahomíra Faktorová:** Methodology, Investigation, Writing – review & editing, Visualization. **Anton Horváth:** Writing – review & editing, Funding acquisition. **Gertraud Burger:** Investigation, Writing – review & editing, Funding acquisition. **Julius Lukeš:** Writing – review & editing, Project administration, Funding acquisition. **Ingrid Škodová-Sveráková:** Conceptualization, Methodology, Investigation, Writing – original draft, Visualization, Project administration, Funding acquisition.

Declaration of Competing Interest

The authors declare that they have no conflicts of interest with the contents of this article.

Data availability

The mass spectrometry proteomics data were deposited to the ProteomeXchange Consortium via the PRIDE partner repository [74] with the dataset identifiers PXD035043 (E3 IP) and PXD035104 (subcellular fractions; 10.6019/PXD035104).

Acknowledgements

We thank Aleš Horák (Institute of Parasitology) for sharing unpublished data. This work was supported by grants from the Czech Grant Agency (23-06479X to J.L.), the Gordon and Betty Moore Foundation (#9354 to J.L.), the ERD project (16_019/0000759 and 313011W428 to J.L.), and e-INFRA CZ (ID:90140), the de Duve Institute (to F.R.O.), Scientific Grant Agency of the Slovak Ministry of Education and the Academy of Sciences (VEGA 1/0553/21 to A.H. and 1/0781/19 to I.Š. S.), Slovak Research and Development Agency Contracts (APVV-20-0129 to A.H.), the ACCORD project co-financed by the ERDF (ITMS2014+: 313021X329), the ERDF project Center for Biomedical Research – BIOMEDIRES – II. stage (313011W428 to P.B.), the Natural Sciences and Engineering Research Council of Canada (NSERC; grant RGPIN-2019-04024 to G.B.), and the Fonds de Recherche du Québec—Nature et Technologies (FRQNT; grant 2023-PR-326068 to G. B.).

Appendix A. Supplementary data

Supplementary data to this article can be found online at https://doi.org/10.1016/j.bbagen.2023.130419.

References

[1] E. Meléndez-Hevia, T.G. Waddell, M. Cascante, The puzzle of the Krebs citric acid cycle: assembling the pieces of chemically feasible reactions, and opportunism in the design of metabolic pathways during evolution, J. Mol. Evol. 43 (1996) 293–303, https://doi.org/10.1007/BF02338838.

[2] H. Kagamiyama, H. Hayashi, Branched-chain amino-acid aminotransferase of *Escherichia coli*, Methods Enzymol. 324 (2000) 103–113, https://doi.org/10.1016/s0076-6879(00)24223-7.

[3] J. Škerlová, J. Berndtsson, H. Nolte, M. Ott, P. Stenmark, Structure of the native pyruvate dehydrogenase complex reveals the mechanism of substrate insertion, Nat. Commun. 12 (2021) 5277, https://doi.org/10.1038/s41467-021-25570-y.

[4] S.S. Mande, S. Sarfaty, M.D. Allen, R.N. Perham, W.G.J. Hol, Protein-protein interactions in the pyruvate dehydrogenase multienzyme complex: dihydrolipoamide dehydrogenase complexed with the binding domain of dihydrolipoamide acetyltransferase, Structure. 4 (1996) 277–286, https://doi.org/10.1016/S0969-2126(96)00032-9.

[5] G.E. Schulz, R.H. Schirmer, W. Sachsenheimer, E.F. Pai, The structure of the flavoenzyme glutathione reductase, Nature. 273 (1978) 120–124, https://doi.org/10.1038/273120a0.

[6] J. Kuriyan, T.S.R. Krishna, L. Wong, B. Guenther, A. Pahler, C.H. Williams, P. Model, Convergent evolution of similar function in two structurally divergent enzymes, Nature. 352 (1991) 172–174, https://doi.org/10.1038/352172a0.

[7] J. Kuriyan, X.P. Kong, T.S.R. Krishna, R.M. Sweet, N.J. Murgolo, H. Field, A. Cerami, G.B. Henderson, X-ray structure of trypanothione reductase from *Crithidia fasciculata* at 2.4-Å resolution, Proc. Natl. Acad. Sci. U. S. A. 88 (1991) 8764–8768, https://doi.org/10.1073/pnas.88.19.8764.

[8] N. Schiering, W. Kabsch, M.J. Moore, M.D. Distefano, C.T. Walsh, E.F. Pai, Structure of the detoxification catalyst mercuric ion reductase from *Bacillus* sp. strain RC607, Nature. 352 (1991) 168–172, https://doi.org/10.1038/352168a0.

[9] S.J. Sanderson, S.S. Khan, R.G. McCartney, C. Miller, J.G. Lindsay, Reconstitution of mammalian pyruvate dehydrogenase and 2-oxoglutarate dehydrogenase complexes: analysis of protein X involvement and interaction of homologous and heterologous dihydrolipoamide dehydrogenases, Biochem. J. 319 (1996) 109–116, https://doi.org/10.1042/bj3190109.

[10] X.Y. Pei, C.M. Titman, R.A.W. Frank, F.J. Leeper, B.F. Luisi, Snapshots of catalysis in the E1 subunit of the pyruvate dehydrogenase multienzyme complex, Structure. 16 (2008) 1860–1872, https://doi.org/10.1016/j.str.2008.10.009.

[11] E.R. Butterfield, C.J. Howe, R.E.R. Nisbet, An analysis of dinoflagellate metabolism using EST data, Protist. 164 (2013) 218–236, https://doi.org/10.1016/j.protis.2012.09.001.

[12] M.E. Schreiner, D. Fiur, J. Holátko, M. Pátek, B.J. Eikmanns, E1 enzyme of the pyruvate dehydrogenase complex in *Corynebacterium glutamicum*: molecular analysis of the gene and phylogenetic aspects, J. Bacteriol. 187 (2005) 6005–6018, https://doi.org/10.1128/JB.187.17.6005-6018.2005.

[13] M. Rahmatullah, S. Gopalakrishnan, P.C. Andrews, C.L. Chang, G.A. Radke, T. E. Roche, Subunit associations in the mammalian pyruvate dehydrogenase complex. Structure and role of protein X and the pyruvate dehydrogenase component binding domain of the dihydrolipoyl transacetylase component, J. Biol. Chem. 264 (1989) 2221–2227.

[14] J.R. Sokatch, V. McCully, C.M. Roberts, Purification of a branched-chain keto acid dehydrogenase from *Pseudomonas putida*, J. Bacteriol. 148 (1981) 647–652, https://doi.org/10.1128/jb.148.2.647-652.1981.

[15] N.S. Nemeria, G. Gerfen, P.R. Nareddy, L. Yang, X. Zhang, M. Szostak, F. Jordan, The mitochondrial 2-oxoadipate and 2-oxoglutarate dehydrogenase complexes share their E2 and E3 components for their function and both generate reactive oxygen species, Free Radic. Biol. Med. 115 (2018) 136–145, https://doi.org/10.1016/j.freeradbiomed.2017.11.018.

[16] A.H. Millar, S.A. Hill, C.J. Leaver, Plant mitochondrial 2-oxoglutarate dehydrogenase complex: purification and characterization in potato, Biochem. J. Pt 2 (1999) 327–334, https://doi.org/10.1042/0264-6021:3430327.

[17] M. Hoffelder, K. Raasch, J. Van Ooyen, L. Eggeling, The E2 domain of OdhA of *Corynebacterium glutamicum* has succinyltransferase activity dependent on lipoyl residues of the acetyltransferase AceF, J. Bacteriol. 192 (2010) 5203–5211, https://doi.org/10.1128/JB.00597-10.

[18] A. Niebisch, A. Kabus, C. Schultz, B. Weil, M. Bott, Corynebacterial protein kinase G controls 2-oxoglutarate dehydrogenase activity via the phosphorylation status of the OdhI protein, J. Biol. Chem. 281 (2006) 12300–12307, https://doi.org/10.1074/jbc.M512515200.

[19] E.M. Bruch, P. Vilela, L. Yang, A. Boyko, N. Lexa-Sapart, B. Raynal, P.M. Alzari, M. Bellinzoni, Actinobacteria challenge the paradigm: a unique protein architecture for a well-known, central metabolic complex, Proc. Natl. Acad. Sci. U. S. A. 118 (2021), e2112107118, https://doi.org/10.1073/pnas.2112107118.

[20] R.N. Perham, Swinging arms and swinging domains in multifunctional enzymes: catalytic machines for multistep reactions, Annu. Rev. Biochem. 69 (2000) 961–1004, https://doi.org/10.1146/annurev.biochem.69.1.961.

[21] F. Seeber, J. Limenitakis, D. Soldati-Favre, Apicomplexan mitochondrial metabolism: a story of gains, losses and retentions, Trends Parasitol. 24 (2008) 468–478, https://doi.org/10.1016/j.pt.2008.07.004.

[22] R.D. Oppenheim, D.J. Creek, J.I. Macrae, K.K. Modrzynska, P. Pino, J. Limenitakis, V. Polonais, F. Seeber, M.P. Barrett, O. Billker, M.J. McConville, D. Soldati-Favre, BCKDH: The missing link in apicomplexan mitochondrial metabolism is required for full virulence of *Toxoplasma gondii* and *Plasmodium berghei*, PLoS Pathog. 10 (2014), e1004263, https://doi.org/10.1371/journal.ppat.1004263.

[23] X.W.A. Chan, C. Wrenger, K. Stahl, B. Bergmann, M. Winterberg, I.B. Müller, K. J. Saliba, Chemical and genetic validation of thiamine utilization as an antimalarial drug target, Nat. Commun. 4 (2013) 2060, https://doi.org/10.1038/ncomms3060.

[24] N.S. Nemeria, G. Gerfen, L. Yang, X. Zhang, F. Jordan, Evidence for functional and regulatory cross-talk between the tricarboxylic acid cycle 2-oxoglutarate dehydrogenase complex and 2-oxoadipate dehydrogenase on the L-lysine, L-hydroxylysine and L-tryptophan degradation pathways from studies in vitro, Biochim. Biophys. Acta Bioenerg. 2018 (1859) 932–939, https://doi.org/10.1016/j.bbabio.2018.05.001.

[25] A. Butenko, F.R. Opperdoes, O. Flegontova, A. Horák, V. Hampl, P. Keeling, R.M. R. Gawryluk, D. Tikhonenkov, P. Flegontov, J. Lukeš, Evolution of metabolic capabilities and molecular features of diplonemids, kinetoplastids, and euglenids, BMC Biol. 18 (2020) 23, https://doi.org/10.1186/s12915-020-0754-1.

[26] D. Tashyreva, A.G.B. Simpson, G. Prokopchuk, I. Škodová-Sveráková, A. Butenko, M. Hammond, E.E. George, O. Flegontova, K. Záhonová, D. Faktorová, A. Yabuki, A. Horák, P.J. Keeling, J. Lukeš, Diplonemids – a review on "new" flagellates on the oceanic block, Protist. 173 (2022), 125868, https://doi.org/10.1016/j.protis.2022.125868.

[27] A.Y. Kostygov, A. Karnkowska, J. Votýpka, D. Tashyreva, K. Maciszewski, V. Yurchenko, J. Lukeš, Euglenozoa: taxonomy, diversity and ecology, symbioses and viruses, Open Biol. 11 (2021), 200407, https://doi.org/10.1098/rsob.200407.

[28] D. Faktorová, B. Kaur, M. Valach, L. Graf, C. Benz, G. Burger, J. Lukeš, Targeted integration by homologous recombination enables *in situ* tagging and replacement of genes in the marine microeukaryote *Diplonema papillatum*, Environ. Microbiol. 22 (2020) 3660–3670, https://doi.org/10.1111/1462-2920.15130.

[29] A.K. Panigrahi, A. Zíková, R.A. Dalley, N. Acestor, Y. Ogata, A. Anupama, P. J. Myler, K.D. Stuart, Mitochondrial complexes in *Trypanosoma brucei*: a novel complex and a unique oxidoreductase complex, Mol. Cell. Proteomics 7 (2008) 534–545, https://doi.org/10.1074/mcp.m700430-mcp200.

[30] T.E. Ebenezer, M. Zoltner, A. Burrell, A. Nenarokova, A.M.G. Novák Vanclová, B. Prasad, P. Soukal, C. Santana-Molina, E. O'Neill, N.N. Nankissoor, N. Vadakedath, V. Daiker, S. Obado, S. Silva-Pereira, A.P. Jackson, D.P. Devos, J. Lukeš, M. Lebert, S. Vaughan, V. Hampl, M. Carrington, M.L. Ginger, J.B. Dacks, S. Kelly, M.C. Field, Transcriptome, proteome and draft genome of *Euglena gracilis*, BMC Biol. 17 (2019) 11, https://doi.org/10.1186/s12915-019-0626-8.

[31] S.F. Altschul, W. Gish, W. Miller, E.W. Myers, D.J. Lipman, Basic local alignment search tool, J. Mol. Biol. 215 (1990) 403–410, https://doi.org/10.1016/S0022-2836(05)80360-2.

[32] M. Valach, S. Moreira, C. Petitjean, C. Benz, A. Butenko, O. Flegontova, A. Nenarokova, G. Prokopchuk, T. Batstone, P. Lepébie, L. Lemogo, M. Sarrasin, P. Stretenowich, P. Tripathi, E. Yazaki, T. Nara, B. Henrissat, B.F. Lang, M.W. Gray, T.A. Williams, J. Lukeš, G. Burger, Recent expansion of metabolic versatility in *Diplonema papillatum*, the model species of a highly speciose group of marine eukaryotes, BMC Biol. 21 (2023) 99, https://doi.org/10.1186/s12915-023-01563-9.

[33] M. Valach, S. Moreira, S. Hoffmann, P.F. Stadler, G. Burger, Keeping it complicated: mitochondrial genome plasticity across diplonemids, Sci. Rep. 7 (2017) 14166, https://doi.org/10.1038/s41598-017-14286-z.

[34] B. Kaur, K. Záhonová, M. Valach, D. Faktorová, G. Prokopchuk, G. Burger, J. Lukeš, Gene fragmentation and RNA editing without borders: eccentric mitochondrial genomes of diplonemids, Nucleic Acids Res. 48 (2020) 2694–2708, https://doi.org/10.1093/nar/gkz1215.

[35] K. Záhonová, Z. Füssy, E. Birčák, A.M.G. Novák Vanclová, V. Klimeš, M. Vesteg, J. Krajčovič, M. Oborník, M. Eliáš, Peculiar features of the plastids of the colourless alga *Euglena longa* and photosynthetic euglenophytes unveiled by transcriptome analyses, Sci. Rep. 8 (2018) 17012, https://doi.org/10.1038/s41598-018-35389-1.

[36] P.J. Keeling, F. Burki, H.M. Wilcox, B. Allam, E.E. Allen, L.A. Amaral-Zettler, E. V. Armbrust, J.M. Archibald, A.K. Bharti, C.J. Bell, B. Beszteri, K.D. Bidle, C. T. Cameron, L. Campbell, D.A. Caron, R.A. Cattolico, J.L. Collier, K. Coyne, S. K. Davy, P. Deschamps, S.T. Dyhrman, B. Edvardsen, R.D. Gates, C.J. Gobler, S. J. Greenwood, S.M. Guida, J.L. Jacobi, K.S. Jakobsen, E.R. James, B. Jenkins, U. John, M.D. Johnson, A.R. Juhl, A. Kamp, L.A. Katz, R. Kiene, A. Kudryavtsev, B. S. Leander, S. Lin, C. Lovejoy, D. Lynn, A. Marchetti, G. McManus, A.M. Nedelcu, S. Menden-Deuer, C. Miceli, T. Mock, M. Montresor, M.A. Moran, S. Murray, G. Nadathur, S. Nagai, P.B. Ngam, B. Palenik, J. Pawlowski, G. Petroni, G. Piganeau, M.C. Posewitz, K. Rengefors, G. Romano, M.E. Rumpho, T. Rynearson, K.B. Schilling, D.C. Schroeder, A.G. Simpson, C.H. Slamovits, D.R. Smith, G. J. Smith, S.R. Smith, H.M. Sosik, P. Stief, E. Theriot, S.N. Twary, P.E. Umale, D. Vaulot, B. Wawrik, G.L. Wheeler, W.H. Wilson, Y. Xu, A. Zingone, A.Z. Worden, The Marine Microbial Eukaryote Transcriptome Sequencing Project (MMETSP): illuminating the functional diversity of eukaryotic life in the oceans through transcriptome sequencing, PLoS Biol. 12 (2014), e1001889, https://doi.org/10.1371/journal.pbio.1001889.

[37] G. Lax, M. Kolisko, Y. Eglit, W.J. Lee, N. Yubuki, A. Karnkowska, B.S. Leander, G. Burger, P.J. Keeling, A.G.B. Simpson, Multigene phylogenetics of euglenids based on single-cell transcriptomics of diverse phagotrophs, Mol. Phylogenet. Evol. 159 (2021), 107088, https://doi.org/10.1016/j.ympev.2021.107088.

[38] K. Záhonová, G. Lax, S.D. Sinha, G. Leonard, T.A. Richards, J. Lukeš, J. G. Wideman, Single-cell genomics unveils a canonical origin of the diverse mitochondrial genomes of euglenozoans, BMC Biol. 19 (2021) 103, https://doi.org/10.1186/s12915-021-01035-y.

[39] S.R. Eddy, A new generation of homology search tools based on probabilistic inference, Genome Inf. 23 (2009) 205–211.

[40] P. Jones, D. Binns, H.Y. Chang, M. Fraser, W. Li, C. McAnulla, H. McWilliam, J. Maslen, A. Mitchell, G. Nuka, S. Pesseat, A.F. Quinn, A. Sangrador-Vegas, M. Scheremetjew, S.Y. Yong, R. Lopez, S. Hunter, InterProScan 5: genome-scale protein function classification, Bioinformatics. 30 (2014) 1236–1240, https://doi.org/10.1093/bioinformatics/btu031.

[41] M. Kearse, R. Moir, A. Wilson, S. Stones-Havas, M. Cheung, S. Sturrock, S. Buxton, A. Cooper, S. Markowitz, C. Duran, T. Thierer, B. Ashton, P. Meintjes, A. Drummond, Geneious Basic: an integrated and extendable desktop software platform for the organization and analysis of sequence data, Bioinformatics. 28 (2012) 1647–1649, https://doi.org/10.1093/bioinformatics/bts199.

[42] M.G. Claros, P. Vincens, Computational method to predict mitochondrially imported proteins and their targeting sequences, Eur. J. Biochem. 241 (1996) 779–786, https://doi.org/10.1111/j.1432-1033.1996.00779.x.

[43] Y. Fukasawa, J. Tsuji, S.C. Fu, K. Tomii, P. Horton, K. Imai, MitoFates: improved prediction of mitochondrial targeting sequences and their cleavage sites, Mol. Cell. Proteomics 14 (2015) 1113–1126, https://doi.org/10.1074/mcp.M114.043083.

[44] J.J. Almagro Armenteros, M. Salvatore, O. Emanuelsson, O. Winther, G. von Heijne, A. Elofsson, H. Nielsen, Detecting sequence signals in targeting peptides using deep learning, Life Sci. Alliance. 2 (2019), e201900429, https://doi.org/10.26508/lsa.201900429.

[45] F. Burki, A.J. Roger, M.W. Brown, A.G.B. Simpson, The new tree of eukaryotes, Trends Ecol. Evol. 35 (2020) 43–55, https://doi.org/10.1016/j.tree.2019.08.008.

[46] K. Katoh, D.M. Standley, MAFFT multiple sequence alignment software version 7: improvements in performance and usability, Mol. Biol. Evol. 30 (2013) 772–780, https://doi.org/10.1093/molbev/mst010.

[47] S. Capella-Gutiérrez, J.M. Silla-Martínez, T. Gabaldón, trimAl: a tool for automated alignment trimming in large-scale phylogenetic analyses, Bioinformatics. 25 (2009) 1972–1973, https://doi.org/10.1093/bioinformatics/btp348.

[48] L.T. Nguyen, H.A. Schmidt, A. von Haeseler, B.Q. Minh, IQ-TREE: a fast and effective stochastic algorithm for estimating maximum-likelihood phylogenies, Mol. Biol. Evol. 32 (2015) 268–274, https://doi.org/10.1093/molbev/msu300.

[49] H.-C. Wang, B.Q. Minh, E. Susko, A.J. Roger, Modeling site heterogeneity with posterior mean site frequency profiles accelerates accurate phylogenomic estimation, Syst. Biol. 67 (2018) 216–235, https://doi.org/10.1093/sysbio/syx068.

[50] D.T. Hoang, O. Chernomor, A. von Haeseler, B.Q. Minh, L.S. Vinh, UFBoot2: improving the ultrafast bootstrap approximation, Mol. Biol. Evol. 35 (2017) 518–522, https://doi.org/10.1093/molbev/msx281.

[51] B. Kaur, M. Valach, P. Peña-Diaz, S. Moreira, P.J. Keeling, G. Burger, J. Lukeš, D. Faktorová, Transformation of *Diplonema papillatum*, the type species of the highly diverse and abundant marine microeukaryotes Diplonemida (Euglenozoa), Environ. Microbiol. 20 (2018) 1030–1040, https://doi.org/10.1111/1462-2920.14041.

[52] K. Šubrtová, B. Panicucci, A. Zíková, ATPaseTb2, a unique membrane-bound FoF1-ATPase component, is essential in bloodstream and dyskinetoplastic trypanosomes, PLoS Pathog. 11 (2015), e1004660, https://doi.org/10.1371/journal.ppat.1004660.

[53] M. Valach, A. Léveillé-Kunst, M.W. Gray, G. Burger, Respiratory chain complex I of unparalleled divergence in diplonemids, J. Biol. Chem. 293 (2018) 16043–16056, https://doi.org/10.1074/jbc.RA118.005326.

[54] J. Pyrih, V. Rašková, I. Škodová-Sveráková, T. Pánek, J. Lukeš, ZapE/Afg1 interacts with Oxa1 and its depletion causes a multifaceted phenotype, PLoS One 15 (2020), e0234918, https://doi.org/10.1371/journal.pone.0234918.

[55] J. Cox, M. Mann, MaxQuant enables high peptide identification rates, individualized p.p.b.-range mass accuracies and proteome-wide protein quantification, Nat. Biotechnol. 26 (2008) 1367–1372, https://doi.org/10.1038/nbt.1511.

[56] J. Cox, N. Neuhauser, A. Michalski, R.A. Scheltema, J.V. Olsen, M. Mann, Andromeda: a peptide search engine integrated into the MaxQuant environment, J. Proteome Res. 10 (2011) 1794–1805, https://doi.org/10.1021/pr101065j.

[57] M. Zoltner, G.D. Campagnaro, G. Taleva, A. Burrell, M. Cerone, K.F. Leung, F. Achcar, D. Horn, S. Vaughan, C. Gadelha, A. Zíková, M.P. Barrett, H.P. de Koning, M.C. Field, Suramin exposure alters cellular metabolism and mitochondrial energy production in African trypanosomes, J. Biol. Chem. 295 (2020) 8331–8347, https://doi.org/10.1074/jbc.RA120.012355.

[58] I. Škodová-Sveráková, K. Záhonová, V. Juricová, M. Danchenko, M. Moos, P. Baráth, G. Prokopchuk, A. Butenko, V. Lukáčová, L. Kohútová, B. Bučková, A. Horák, D. Faktorová, A. Horváth, P. Šimek, J. Lukeš, Highly flexible metabolism of the marine euglenozoan protist *Diplonema papillatum*, BMC Biol. 19 (2021) 251, https://doi.org/10.1186/s12915-021-01186-y.

[59] B. Schwanhüusser, D. Busse, N. Li, G. Dittmar, J. Schuchhardt, J. Wolf, W. Chen, M. Selbach, Global quantification of mammalian gene expression control, Nature. 473 (2011) 337–342, https://doi.org/10.1038/nature10098.

[60] P. Čermáková, A. Maďarová, P. Baráth, J. Bellová, V. Yurchenko, A. Horváth, Differences in mitochondrial NADH dehydrogenase activities in trypanosomatids, Parasitology. 148 (2021) 1161–1170, https://doi.org/10.1017/S0031182020002425.

[61] K.P. Block, R. Paul Aftring, M.G. Buse, A.E. Harper, Estimation of branched-chain α-keto acid dehydrogenase activation in mammalian tissues, Methods Enzymol. 166 (1988) 201–213, https://doi.org/10.1016/S0076-6879(88)66026-5.

[62] J.G. McCormack, E.S. Bromidge, N.J. Dawes, Characterization of the effects of Ca2 + on the intramitochondrial Ca2+−sensitive dehydrogenases within intact rat-kidney mitochondria, BBA - Bioenerg. 934 (1988) 282–292, https://doi.org/10.1016/0005-2728(88)90088-6.

[63] D.J. Danner, E.D. Davidson, L.J. Elsas, Thiamine increases the specific activity of human liver branched chain α-ketoacid dehydrogenase, Nature. 254 (1975) 529–530, https://doi.org/10.1038/254529a0.

[64] J.E. Knapp, D.T. Mitchell, M.A. Yazdi, S.R. Ernst, L.J. Reed, M.L. Hackert, Crystal structure of the truncated cubic core component of the *Escherichia coli* 2-oxoglutarate dehydrogenase multienzyme complex, J. Mol. Biol. 280 (1998) 655–668, https://doi.org/10.1006/jmbi.1998.1924.

[65] H. Kinugawa, N. Kondo, A. Komine-Abe, T. Tomita, M. Nishiyama, S. Kosono, In vitro reconstitution and characterization of pyruvate dehydrogenase and 2-oxoglutarate dehydrogenase hybrid complex from *Corynebacterium glutamicum*, Microbiologyopen. 9 (2020), e1113, https://doi.org/10.1002/mbo3.1113.

[66] C. Schnarrenberger, W. Martin, Evolution of the enzymes of the citric acid cycle and the glyoxylate cycle of higher plants, Eur. J. Biochem. 269 (2002) 868–883, https://doi.org/10.1046/j.0014-2956.2001.02722.x.

[67] N.L. Marrott, J.J.T. Marshall, D.I. Svergun, S.J. Crennell, D.W. Hough, M. J. Danson, J.M.H. Van Den Elsen, The catalytic core of an archaeal 2-oxoacid dehydrogenase multienzyme complex is a 42-mer protein assembly, FEBS J. 279 (2012) 713–723, https://doi.org/10.1111/j.1742-4658.2011.08461.x.

[68] A. De Kok, A.F. Hengeveld, A. Martin, A.H. Westphal, The pyruvate dehydrogenase multi-enzyme complex from Gram-negative bacteria, Biochim. Biophys. Acta 1385 (1998) 353–366, https://doi.org/10.1016/S0167-4838(98)00079-X.

[69] M. Smolle, J.G. Lindsay, Molecular architecture of the pyruvate dehydrogenase complex: bridging the gap, Biochem. Soc. Trans. 34 (2006) 815–818, https://doi.org/10.1042/BST0340815.

[70] J. Lee, S. Oh, S. Bhattacharya, Y. Zhang, L. Florens, M.P. Washburn, J.L. Workman, The plasticity of the pyruvate dehydrogenase complex confers a labile structure that is associated with its catalytic activity, PLoS One 15 (2021), e0243489, https://doi.org/10.1371/journal.pone.0243489.

[71] V. Jagannathan, R.S. Schweet, Pyruvic oxidase of pigeon breast muscle. I. Purification and properties of the enzyme, J. Biol. Chem. 196 (1952) 551–562.

[72] H. Oku, T. Kaneda, Biosynthesis of branched-chain fatty acids in *Bacillis subtilis*. A decarboxylase is essential for branched-chain fatty acid synthetase, J. Biol. Chem. 263 (1988) 18386–18396, https://doi.org/10.1016/s0021-9258(19)81371-6.

[73] S. Prajapati, D. Haselbach, S. Wittig, M.S. Patel, A. Chari, C. Schmidt, H. Stark, K. Tittmann, Structural and functional analyses of the human PDH complex suggest a "division-of-labor" mechanism by local E1 and E3 clusters, Structure. 27 (2019) 1124–1136, https://doi.org/10.1016/j.str.2019.04.009.

[74] Y. Perez-Riverol, A. Csordas, J. Bai, M. Bernal-Llinares, S. Hewapathirana, D. J. Kundu, A. Inuganti, J. Griss, G. Mayer, M. Eisenacher, E. Pérez, J. Uszkoreit, J. Pfeuffer, T. Sachsenberg, Ş. Yilmaz, S. Tiwary, J. Cox, E. Audain, M. Walzer, A. F. Jarnuczak, T. Ternent, A. Brazma, J.A. Vizcaíno, The PRIDE database and related tools and resources in 2019: improving support for quantification data, Nucleic Acids Res. 47 (2019) D442–D450, https://doi.org/10.1093/nar/gky1106.